

# Influence of initial conditions on the flow patterns of a shock-accelerated thin fluid layer

John M. Budzinski and Robert F. Benjamin

*Dynamic Experimentation Division, Los Alamos National Laboratory, Los Alamos, New Mexico 87545*

Jeffrey W. Jacobs

*Department of Aerospace and Mechanical Engineering, University of Arizona, Tucson, Arizona 85721*

(Received 5 May 1994; accepted 22 July 1994)

Previous observations of three flow patterns generated by shock acceleration of a thin perturbed, fluid layer are now correlated with asymmetries in the initial conditions. Using a different diagnostic (planar laser Rayleigh scattering) than the previous experiments, upstream mushrooms, downstream mushrooms, and sinuous patterns are still observed. For each experiment the initial perturbation amplitude on one side of the layer can either be larger, smaller, or the same as the amplitude on the other side, as observed with two images per experiment, and these differences lead to the formation of the different patterns.

This study is directed toward a better understanding of the flow of an accelerated heavy layer imbedded between lower-density fluids. As an example, this phenomenon may occur in inertial confinement fusion targets when the ablatively driven impulse causes implosion of a fuel-containing shell. A potential difficulty is the mixing of shell material with the fuel, as a consequence of interfacial fluid instability.

A shock-accelerated layer involves the Richtmyer-Meshkov (RM) instability<sup>1,2</sup> of each interface between fluids of different density. A perturbed interface between two fluids subjected to a normal, impulsive acceleration is unstable and distorts after the interaction. If the downstream fluid is denser than the upstream fluid the perturbation grows. However, if the upstream fluid is denser than the downstream fluid, the perturbation first reverses phase and then grows, and the original peaks in the perturbation will become the valleys and the valleys will become the peaks. In both cases the early-time growth rate is constant and proportional to the amplitude of the initial perturbation. At later times the growth rate decreases, and mushroom shapes form from the peaks in the distorting interface.

We study a shock interaction with a layer of heavy gas bounded on both sides by a lighter gas, where both interfaces of the layer have nearly sinusoidal perturbations. Previous research<sup>3,4</sup> observed that three distinct flow patterns evolve from similar initial conditions, and speculated that differences in initial conditions might influence which flow pattern occurs during each event. These experiments observed only the dynamic flow condition for each event at one preset time because of limitations that precluded multiple image acquisition. We now report experiments where both initial and dynamic flow conditions are recorded for each event. The same three flows are observed, and have a strong correlation with asymmetries in the initial flow profile.

The present experiments use planar laser Rayleigh scattering (PLRS)<sup>5</sup> to capture two frames per event, but use the same shock tube and test section as in the earlier work.<sup>3,4</sup> Our PLRS images clearly show regions of high SF<sub>6</sub> concentration because SF<sub>6</sub> scatters about six times more light than air. Two pulsed dye lasers illuminate the test region with

coplanar sheets of laser light, and a cooled CCD camera records each image. We convert the images to maps of SF<sub>6</sub> concentration by calibrating the system with scattering from pure air and pure SF<sub>6</sub>.

The nozzle above the test section produces a vertically flowing, laminar gas jet<sup>6</sup> (i.e., the gas curtain) with a varicose cross section and diffuse boundaries; the wavelength is about 6 mm and the peak-to-peak amplitude is up to 2 mm on each side. This flow system has been shown to produce a two-dimensional flow.<sup>4</sup> The shock tube is fired when the gas curtain appears to be stable as observed with a real time schlieren system, and drives a Mach 1.2 shock wave in air. Small, unsteady, uncontrollable fluctuations in the SF<sub>6</sub> flow cause asymmetries which vary from experiment to experiment and are correlated with the three different shock-accelerated flows. We find that the thicker regions of the layer contain about 50% SF<sub>6</sub> and the thinner regions about 40% SF<sub>6</sub>. The SF<sub>6</sub> concentration across the layer width has an approximately Gaussian profile.

We observe the same three patterns after a Mach 1.2 shock interaction as seen in the earlier work, and find that asymmetries in the initial condition correlate with the three postshock flow patterns in over 90% of the 100+ experiments performed. Typical examples of the initial and dynamic conditions for the three flow patterns are shown in Fig. 1, where the initial condition was taken about 100  $\mu$ s before the shock interaction and the dynamic condition at 400–450  $\mu$ s after the shock interaction. Upstream mushrooms formed in about 46% of the experiments, a sinuous pattern formed in about 41% of the experiments, and downstream mushrooms developed in 13% of the experiments. Mostly we find that an upstream mushroom pattern develops when the perturbations on the upstream side (i.e., on the side first interacting with the shock wave) are larger than the perturbations on the downstream side. A sinuous pattern forms when the perturbations on the downstream side are about the same or slightly larger than upstream side. A downstream mushroom develops when the perturbation on the downstream side is much larger than the perturbation on the upstream side. About 8% of the experimental images were

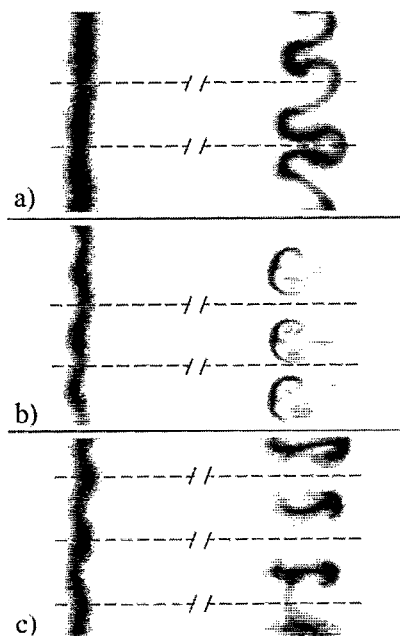


FIG. 1. Composite of images from three typical experiments showing the initial and dynamic condition on each experiment. The shock wave moves left to right. The distance shown in the figure between the initial and dynamic condition of each pair is considerably less than the actual distance in the experiment. Each pair of initial and dynamic condition was recorded on the same event. (a) Sinuous, dynamic image recorded at  $t=450 \mu\text{s}$  after the shock interaction; (b) upstream mushroom, dynamic image  $t=450 \mu\text{s}$ ; (c) downstream mushroom, dynamic image  $t=400 \mu\text{s}$ .

anomalous and did not follow the correlation described above.

The postshock flow pattern was classified visually as one of the three flow patterns based on the asymmetries present in the spacing of the pattern lobes and the  $\text{SF}_6$  mass distribution, using the criteria described in Fig. 2. The precise periodicity shown in the patterns in Fig. 2 was usually not present in the data; irregularities often occurred as shown in the typical data, Fig. 1.

When the initial conditions fell between those that produced one of the standard patterns, typically the postshock pattern had characteristics of more than one pattern. When the initial conditions had a downstream perturbation that was not large enough to produce a full downstream mushroom, and yet not small enough to produce a pure sinuous pattern, then by 0.45 ms after the shock interaction, well-defined stems and caps would not be present, but the pattern would have some characteristics of the early-time downstream mushroom pattern. For example, the dimension  $a$  in Fig. 2 would be greater than  $b$ , but not to the extent as found in the development of a standard downstream mushroom. This pattern was categorized as one of the 41% sinuous patterns.

We also find that the upstream mushrooms are aligned with the thicker parts of the initial layer whereas the downstream mushrooms are aligned with the thinner regions. Thus in the early development of downstream mushrooms, the heavy fluid moves laterally (i.e., normal to the shock direction) from the thicker to the thinner regions; there is less lateral movement of the heavy fluid during the early devel-

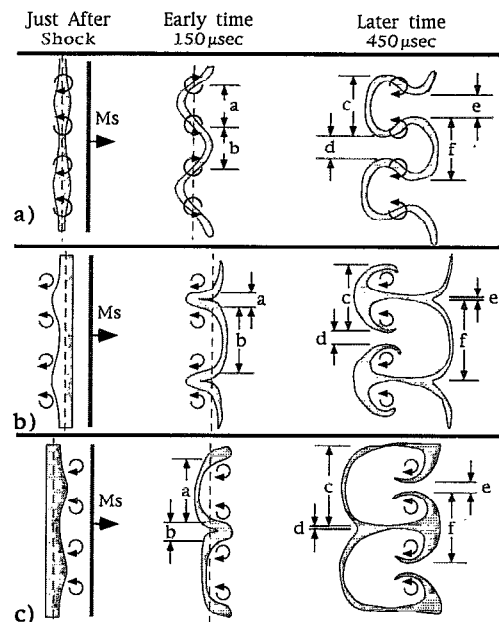


FIG. 2. Differences in the different patterns throughout their development and a simple model to explain why they might occur. (a) Sinuous pattern: perturbations are about equal on both sides of the layer, at early times  $a \sim b$ , at later times  $c \sim e, d \sim f$ , and the  $\text{SF}_6$  is evenly distributed throughout the layer. Just after the shock interaction the center of vorticity (shown by the circular arrows) is roughly in the center of the layer inducing the sinuous pattern to develop. (b) Upstream mushroom pattern: The initial upstream perturbation amplitude is larger than the downstream, at early times  $b > a$ , at later times  $d > e, c < f$ . The highest  $\text{SF}_6$  concentrations and most of the  $\text{SF}_6$  mass is in the mushroom caps. Just after the shock interaction most of the vorticity is to the left of the layer. As the vorticity entrains the fluid the mushrooms form. (c) Downstream mushroom pattern: The initial downstream perturbation amplitude is larger than the upstream. At early times  $a > b$ , at later times  $d < e, c > f$ . The highest  $\text{SF}_6$  concentrations and most of the  $\text{SF}_6$  mass is in the mushroom caps. Just after the shock interaction most of the vorticity is to the right of the layer. As the vorticity entrains the fluid, the mushrooms form.

opment of upstream mushrooms. When a sinuous pattern forms the downstream lobes are aligned with the thin regions of the initial layer and the upstream lobes are aligned with the thicker regions.

Our interpretation of these flow patterns is based on a one-dimensional (1-D) calculation, Richtmyer–Meshkov instability, and vortex dynamics. The wave dynamics of the interaction of a planar shock wave with a layer is complex because of multiple wave–interface interactions. The waves reverberate within the heavy layer after the initial interactions that produce a Mach 1.3 shock wave in the  $\text{SF}_6$  and a Mach 1.17 shock in the air downstream of the layer. The interfaces attain the same velocity after a few reverberations.

The observed nonlinear flow patterns can be interpreted qualitatively as the independent RM-instability growth of each interface, followed by strong coupling in the nonlinear growth regime. Richtmyer's impulse model<sup>1</sup> reasonably predicts the early-time growth rate of a single interface (shown recently in analyses<sup>7,8</sup>). For our layer, the coupling between interfaces is initially weak<sup>7</sup> when perturbation amplitudes are small, so the growth of each interface occurs independently. The impulse model predicts that the ratio of growth rates of the interfaces is equal to the ratio of initial perturbation am-

plitudes because the wavelengths, density ratios, and final velocities are equal. Consequently, the interface with the larger amplitude will initially grow faster. This interface apparently dominates the nonlinear flow, as manifest by mushroom formation on the side with initially larger perturbation. Supporting this view is the observation that upstream mushroom caps are aligned with initially thicker regions of SF<sub>6</sub>, and downstream mushroom caps are aligned with thinner regions, as expected from the phase reversal property of RM instability. It is worth noting that if the interfaces remained weakly coupled in the nonlinear growth stage, one would expect to see postshock flow patterns with both upstream and downstream mushrooms in each experiment. Because these patterns are not observed, it appears that strong interface coupling in the nonlinear growth stage inhibits the formation of mushrooms on the side with initially smaller amplitude.

A complementary explanation for the observed flow patterns is based on viewing the flow evolution from the context of vortex dynamics. The vorticity ( $\omega$ ) is generated baroclinically by the shock interaction through the misalignment of pressure ( $P$ ) and density ( $\rho$ ) gradients:

$$\frac{D}{Dt} \left( \frac{\omega}{\rho} \right) = \frac{1}{\rho^3} \nabla \rho \times \nabla P + \text{nonbaroclinic terms.}$$

The dynamics of this vorticity then generates the growth of the layer. The magnitude of vorticity will be greatest where the pressure and density gradients are most misaligned. Assuming the pressure gradients are predominantly from planar waves,<sup>9</sup> most of the vorticity is expected to be in the regions between the peaks and valleys of initial perturbations. This vorticity distribution is similar to what would be generated by a linear array of cylindrical jets spaced so closely that substantial overlap occurs. This perspective enables comparison between the present study and flows of shock-accelerated cylindrical jets and bubbles.<sup>5,6,10-13</sup> Convective roll-up (i.e., the formation of spiral- or mushroom-shaped patterns) is a prominent feature of flow induced by shocking a cylindrical fluid, as it is here, and indeed such patterns in vorticity-dominated flows are well known. A novel feature of the present work is the apparent competition of vorticity distributions on each side of the layer, and the subsequent collective flow behavior.

The different postshock flows can be understood qualitatively by considering the differences in the vorticity production and transport during and immediately following shock acceleration. When the perturbation amplitude is greater on one side of the layer, more vorticity is generated on that side. Furthermore, the vorticity is preferentially generated in the lighter fluid, as seen by the density weighting in the vorticity equation. This effect accentuates the offset of the vorticity from the center of the layer. These effects are approximated in Fig. 2 by representing the postshock vortic-

ity field by a row of vortices of alternating sign and offset from the center of the layer. The offset is shown exaggerated to emphasize the point. The mushrooms form on the side with the largest initial perturbation amplitude because the heavy fluid is asymmetrically entrained into the side with the most vorticity. The vorticity distribution of a symmetrically perturbed initial layer would be centered on the heavy layer and thus produce a sinuous pattern.

Multiple framing enables the correlation of initial perturbations with the appearance of each of the three distinct flow patterns induced by shock accelerating a thin varicose layer with perturbations on both sides. Mushroom patterns form on the side with larger initial perturbation. These patterns can be understood by the complementary viewpoints of Richtmyer–Meshkov instability at each interface, and the baroclinic generation of vorticity followed by vortex dynamics domination of the flow evolution.

## ACKNOWLEDGMENTS

We acknowledge the continued encouragement of Harold Rogers and the technical support of Bob Critchfield. The work was performed under the auspices of U.S. Department of Energy Contract No. W-7405-ENG-36.

- <sup>1</sup>R. D. Richtmyer, "Taylor instability in shock acceleration of compressible fluids," *Commun. Pure Appl. Math.* **13**, 297 (1960).
- <sup>2</sup>E. E. Meshkov, "Instability of the interface of two gases accelerated by a shock wave," *Izv. Akad. Nauk. SSSR Mekh. Zhidk. Gaza* **4**, 151 (1969) [*Fluid Dyn.* **4**, 101 (1969)].
- <sup>3</sup>J. W. Jacobs, D. L. Klein, D. G. Jenkins, and R. F. Benjamin, "Instability growth patterns of a shock-accelerated thin fluid layer," *Phys. Rev. Lett.* **70**, 583 (1993).
- <sup>4</sup>J. W. Jacobs, D. G. Jenkins, D. L. Klein, and R. F. Benjamin, "Nonlinear growth of shock-accelerated instability in a thin fluid layer," to appear in *J. Fluid Mech.*
- <sup>5</sup>J. M. Budzinski, "Planar Rayleigh scattering measurements of shock enhanced mixing," Ph.D. thesis, California Institute of Technology, 1992.
- <sup>6</sup>J. W. Jacobs, "Shock-induced mixing of a light-gas cylinder," *J. Fluid Mech.* **234**, 629 (1992).
- <sup>7</sup>K. O. Mikaelian, "Growth rate of Richtmyer–Meshkov instability at shocked interfaces," *Phys. Rev. Lett.* **71**, 2903 (1993).
- <sup>8</sup>J. W. Grove, R. Holmes, D. H. Sharp, Y. Yang, and Q. Zhang, "Quantitative theory of Richtmyer–Meshkov instability," *Phys. Rev. Lett.* **71**, 3473 (1993).
- <sup>9</sup>X. Yang, N.J. Zabusky, and I-L. Chern, "'Breakthrough' via dipolar-vortex/jet formation in shock-accelerated density-stratified layers," *Phys. Fluids A* **2**, 892 (1990).
- <sup>10</sup>F. E. Marble, G. J. Hendricks, and E. E. Zukoski, "Progress toward shock enhancement of supersonic combustion processes," *AIAA/SAE/ASME/ASEE 23rd Joint Propulsion Conference*, San Diego, California, AIAA Paper No. 87-1880, 1987.
- <sup>11</sup>J.-F. Haas, and B. Sturtevant, "Interaction of weak shock waves with cylindrical and spherical gas inhomogeneities," *J. Fluid Mech.* **181**, 41 (1987).
- <sup>12</sup>J. M. Picone, and J. P. Boris, "Vorticity generation by shock propagation through bubbles in a gas," *J. Fluid Mech.* **189**, 23 (1988).
- <sup>13</sup>J. Yang, "An analytical and computational investigation of shock-induced vortical flows with applications to supersonic combustion," Ph.D. thesis, California Institute of Technology, 1991.